Optics and Lasers in Engineering 74 (2015) 67–74

Contents lists available at ScienceDirect

Optics and Lasers in Engineering

journal homepage: www.elsevier.com/locate/optlaseng

Patterning of Aluminium thin film on polyethylene terephthalate by multi-beam picosecond laser

Y. Jin [a], W. Perrie [a,*], P. Harris [b], O.J. Allegre [a], K.J. Abrams [c], G. Dearden [a]

[a] Laser Group, Department of Engineering, University of Liverpool, L69 3GQ, UK
[b] The Wolfson Centre for Materials Processing, Brunel University, Uxbridge, Middlesex UB8 3PH, UK
[c] Nanoinvestigation Centre at Liverpool, University of Liverpool, L69 3GQ, UK

ARTICLE INFO

Article history:
Received 13 November 2014
Received in revised form
13 March 2015
Accepted 3 April 2015

Keywords:
Picosecond laser
Spatial light modulator
Ablation
Computer Generated Hologram
Thin film patterning

ABSTRACT

High speed patterning of a 30 nm thick Aluminium thin film on a flexible Polyethylene Terephthalate substrate was demonstrated with the aid of Computer Generated Holograms (CGH's) applied to a phase only Spatial Light Modulator. Low fluence picosecond laser pulses minimise thermal damage to the sensitive substrate and thus clean, single and multi-beam, front side thin film removal is achieved with good edge quality. Interestingly, rear side ablation shows significant Al film delamination. Measured front and rear side ablation thresholds were $F_{th}=0.20\pm0.01$ J cm^{-2} and $F_{th}=0.15\pm0.01$ J cm^{-2} respectively. With laser repetition rate of 200 kHz and 8 diffractive spots, a film removal rate of $R>0.5$ cm^2 s^{-1} was demonstrated during patterning with a fixed CGH and 5 W average laser power. The effective laser repetition rate was $f_{eff}\sim1.3$ MHz. The application of 30 stored CGH's switching up to 10 Hz was also synchronised with motion control, allowing dynamic large area multi-beam patterning which however, slows micro-fabrication.

1. Introduction

Thin film metal patterning of Cu, Au, Ag and Pt using picosecond and nanosecond solid state and UV Excimer lasers on polymers such as polyethylene terephthalate (PET), polyimide, polyethylene naphthalate (PEN) and poly methyl methacrylate (PMMA) is employed in the fabrication of displays, RFID antennae, bio-sensors, photomasks and micro-fluidic devices [1,2].

Thin metal film ablation with ultrashort (fs/ps) laser pulses goes back almost two decades. Pronko et al [3] studied micro-structuring of 600 nm thick Ag deposited on glass with fs, ps and ns laser pulses. Measured ablation threshold, $F_{th}\sim0.3$ Jcm^{-2} was independent of temporal pulselength, from $\tau_p=0.15$–7 ps, consistent with calculations showing that heat diffusion length at $\tau_p=7$ ps was equal to the optical penetration depth. By using the tip of the 6 μm diameter Gaussian focal spot, they produced 300 nm wide, 50 nm deep blind holes at pulselength $\tau_p=200$ fs. Hostetler et al [4] used a femtosecond pump–probe method to determine the electron–phonon coupling constants (g_{e-ph} and hence electron-lattice heating time) in Au, Cr and Al thin films with a range of grain sizes. Al film thickness was $t=13$ nm and measured coupling strength $g_{e-ph}\sim2.2$. 10^{11} W cm^{-3} K^{-1} was almost independent of grain size, with e-phonon coupling time ~ few ps.

Doerr [5] studied ablation of 20 nm thick Aluminium film on fused silica with temporal pulse lengths from 250 fs to 6 ns at $\lambda=400$ nm and high NA=0.85. Ablation threshold was measured to be $F_{th}=0.18$ J cm^{-2} at $\tau_p=2$ ps pulselength while just below F_{th}, nanoscale bumps could also be produced. Such nanobumps and nanojets were previously observed during fs nanostructuring of Au films [6]. A study of femtosecond ablation of Au and Ni films with varying thickness [7] demonstrated the importance of electron diffusion length, determined by g_{e-ph}. Threshold ablation fluence rose linearly with film thickness, saturating at thickness $d\sim50$ nm in Ni whereas in Au, which has a much lower g_{e-ph}, the threshold ablation fluence saturated at $d\sim500$ nm. Sub-wavelength nanostructuring of 100 nm thick Cr film on glass with fs pulses and 0.5NA Schwarzchild objective was demonstrated using the tip of a Gaussian beam by Korte et al [8].

Optical, electrical, and barrier properties of evaporated Al films of different thicknesses (and hence OD's) on flexible PET was studied by Copeland and Astbury [9], and McClure and Copeland [10]. This work clearly demonstrated the temporal change of optical thin film transmission after coating due to the reaction of atmospheric oxygen at the air/Al interface and chemical reaction at the Al/PET interface.

Aluminium on PET has recently been identified as a low cost replacement for printed silver back-electrodes in AC electroluminescent displays (ACEL) which have a number of niche applications, such as back-lights for instruments in cars, aeroplanes, mobile phones,

* Correspondence to: Lairdside Laser Engineering Centre, Campbeltown Road, Birkenhead, Merseyside, CH41 9HP, UK. Tel.: +44 151 650 2305.
E-mail address: wpfemto1@liv.ac.uk (W. Perrie).

http://dx.doi.org/10.1016/j.optlaseng.2015.04.006
0143-8166/

illuminated displays for advertising and safety lights [11]. Their advantages are that they provide a distributed, uniform light sources, they can be made very thin ($<$ 60 μm) and thus flexible and robust. They can also be printed onto virtually any flat substrate. Aluminium-coated films are used in bulk packaging applications, as a barrier layer to both oxygen and water vapour [9] and are available at very low cost.

Single beam micro-structuring can be wasteful of available pulse energy when significant beam attenuation is required. However, the use of very high repetition rate, (MHz), high power, low pulse energy laser systems requiring fast, accurate scanners and tight synchronisation can improve this situation greatly [12]. In the present work, single beam patterning with a low NA lens requires a few μJ's to evaporate the Aluminium film whose thickness is only a few times the optical penetration depth ($l_{opt}\sim 7$ nm at $\lambda=532$ nm). As available pulse energy ($E_P\sim 35$ μJ) was much greater, throughput is improved significantly with diffractive multiple beams created by a Spatial Light Modulator (SLM) addressed with appropriate Computer Generated Holograms (CGH's). Combined with scanning and accurate laser gating, this allowed much faster, high quality patterning, which was the primary aim of the present work. Also, dynamic patterning is demonstrated by running CGH's in real time, synchronised to the galvo scanner and motion control system, demonstrating the flexibility of dynamic masks.

2. Experimental method and materials

A schematic of the experimental system is shown in Fig. 1. The horizontally polarised output beam from a Coherent Talisker (532 nm, 10 ps, 0–200 kHz, 8 W) is expanded $\times 3$ (Jenoptic) then directed to a phase only SLM (Hamamatsu X-10468-04) addressed with appropriate CGH's created in an interactive Labview environment. Optimised phase CGH's were created with the Gerchberg–Saxton (GS) algorithm [13] which yields good diffraction efficiency while minimising energy non-uniformity between beams. A 4f optical system ($f_1=f_2=400$ mm, 1:1 telescope) re-images diffracted multi-beams to the input aperture of the scanning galvo (Aerotech Nmark AGV-14HP) with 250 mm f-theta lens (Linos). The distance from the surface of the SLM to the input aperture of the Galvo was therefore close to $4f_1\sim 1.6$ m. Al/PET samples (30 nm/20 μm) were supported on a flat, 10 mm thick perspex plate, allowing any transmitted laser light to diverge below the substrate. This assembly was supported on a precision 3-axis (x,y, z) motion control system (Aerotech, A3200 Ndrive). The Aerotech Nmark AGV galvo scanner was combined with an Nmark CLS controller. This galvo has high resolution optical encoders allowing Position Synchronised Output (PSO) triggering such that laser gating is synchronised to galvo mirror positions, allowing precise pointing of laser spots on target at the substrate, even when using ms^{-1} scan speeds. Real time application of CGH's was also synchronised with motion control.

3. Results

Surface roughness of the Al on PET and the PET (after low fluence film ablation) was measured using a Wyko NT1100 white light interferometer and found to be, R_a (Al/PET)$=62\pm 4$ nm, R_a (PET)$=55\pm 2$ nm respectively, (Fig. 2). Hence, the slightly reduced surface roughness on the laser exposed PET is consistent with minimal damage to the sensitive substrate. A view through the exposed PET with visible light illumination confirmed optical transparency. The edge between Al/PET and exposed PET is shown in Fig. 2(c), showing a melt burr, approximately 1 μm in height.

3.1. Single pulse ablation threshold

Fig. 3(a–f) shows optical images of front and rear side single pulse ablation of Al film over a fluence range of $0.3<F<1.5$ J cm^{-2}. A comparison of single ablated spots shows that the film curls over at the edges and that this delamination is worse with rear side ablation, Fig. 3(e–h). Clear front and rear side PET damage appears at 1.5 and 0.6 J cm^{-2} respectively.

Fig. 4(a and c) shows SEM images of single pulse front and back side film ablation confirming that the delamination occuring at the film edge is more severe with back side illumination. Elemental analysis usng EDX of ablated regions also confirms the complete removal of Al from PET, Fig. 4(b).

Fig. 5 shows a graph of the measured ablated film diameter squared versus ln E_P for both front and rear side ablation with excellent fits to the data. Results indicate a lower ablation threshold for rear side exposure. The measured front and rear side ablation threshold energy is $E_{p,th}=0.69$ μJ and 0.50 μJ respectively. The gradient ($2\omega_0^2$) yields the $1/e^2$ focal spot diameter to be $2\omega_0\sim 29.7$ μm and ablation thresholds $F_{th}=0.20\pm 0.01$ J cm^{-2} (front) and $F_{th}=0.15\pm 0.01$ J cm^{-2} (rear) respectively. The quoted errors are estimated by allowing variation of the gradient fits to the data. The lower threshold for rear side ablation is not unexpected, since direct heating of the interface between Al and PET (transparent) occurs with this geometry. As pulse energy is increased further, damage to the PET is observed. Included is data on the front side ablation of the PET, with damage threshold $E_{p,th\ PET}=4.06$ μJ and fluence threshold $F_{th,PET}=1.2$ J cm^{-2}. A clear energy window for removing the Aluminium film without significant damage to the PET substrate thus exists.

3.2. Single beam scribing (front)

To achieve continuous scribing, a reasonable pulse overlap is required. Fig. 6(a–f) shows the effect of varying pulse overlap at laser frequencies $f=1$ kHz, 10 kHz and 100 kHz repetition rate with pulse energy $E_P=3$ μJ. A straight edge was obtained when pulse overlap $N\geq 5$ but too high an overlap appeared to create

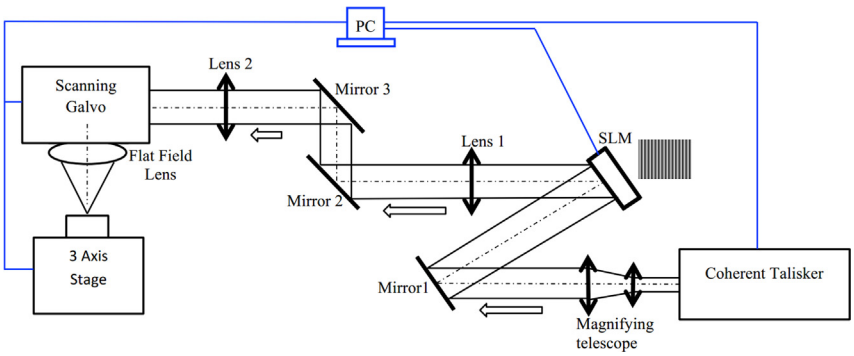

Fig. 1. Schematic of experimental set-up, showing synchronous control of scanner, CGH application to SLM and laser gating.